

Performance and Diagnostic Evaluation of Ozone Predictions by the Eta-Community Multiscale Air Quality Forecast System during the 2002 New England Air Quality Study

Shaocai Yu

Atmospheric Sciences Modeling Division, National Exposure Research Laboratory, U.S. Environmental Protection Agency, Research Triangle Park, NC; and on assignment from Science and Technology Corporation, Hampton, VA

Rohit Mathur

Atmospheric Sciences Modeling Division, Air Resources Laboratory, National Oceanic and Atmospheric Administration, Research Triangle Park, NC; in partnership with the National Exposure Research Laboratory, U.S. Environmental Protection Agency, Research Triangle Park, NC

Daiwen Kang

Atmospheric Sciences Modeling Division, National Exposure Research Laboratory, U.S. Environmental Protection Agency, Research Triangle Park, NC; and on assignment from Science and Technology Corporation, Hampton, VA

Kenneth Schere, Brian Eder, and Jonathan Pleim

Atmospheric Sciences Modeling Division, Air Resources Laboratory, National Oceanic and Atmospheric Administration, Research Triangle Park, NC; in partnership with the National Exposure Research Laboratory, U.S. Environmental Protection Agency, Research Triangle Park, NC

ABSTRACT

A real-time air quality forecasting system (Eta-Community Multiscale Air Quality [CMAQ] model suite) has been developed by linking the National Centers for Environmental Estimation Eta model to the U.S. Environmental Protection Agency (EPA) CMAQ model. This work presents results from the application of the Eta-CMAQ modeling system for forecasting ozone (O_3) over the Northeastern United States during the 2002 New England Air Quality Study (NEAQS). Spatial and temporal performance of the Eta-CMAQ model for O_3 was evaluated by comparison with observations from the

EPA Air Quality System (AQS) network. This study also examines the ability of the model to simulate the processes governing the distributions of tropospheric O_3 on the basis of the intensive datasets obtained at the four Atmospheric Investigation, Regional Modeling, Analysis, and Estimation (AIRMAP) and Harvard Forest (HF) surface sites. The episode analysis reveals that the model captured the buildup of O_3 concentrations over the northeastern domain from August 11 and reproduced the spatial distributions of observed O_3 very well for the daytime (8:00 p.m.) of both August 8 and 12 with most of normalized mean bias (NMB) within $\pm 20\%$. The model reproduced 53.3% of the observed hourly O_3 within a factor of 1.5 with NMB of 29.7% and normalized mean error of 46.9% at the 342 AQS sites. The comparison of modeled and observed lidar O_3 vertical profiles shows that whereas the model reproduced the observed vertical structure, it tended to overestimate at higher altitude. The model reproduced 64–77% of observed NO_2 photolysis rate values within a factor of 1.5 at the AIRMAP sites. At the HF site, comparison of modeled and observed O_3 /nitrogen oxide (NO_x) ratios suggests that the site is mainly under strongly NO_x -sensitive conditions ($>53\%$). It was found that the modeled lower limits of the O_3 production efficiency values (inferred from O_3 -CO correlation) are close to the observations.

IMPLICATIONS

Air quality forecast simulations over the Northeastern United States with the Eta-CMAQ system are evaluated against a variety of measurements from the 2002 NEAQS. The model captured the hourly variations and broad synoptic and inter-day variations seen in the observations of different gas species. In light of uncertainties in current photochemical mechanisms and specification of real-time emission estimates and prognostic meteorological fields, the model performance for O_3 in forecast mode can be considered to be reasonable.

INTRODUCTION

O₃, a secondary pollutant, is created in part by pollution from anthropogenic and biogenic sources. The daily maximum 8-hr National Ambient Air Quality Standards (NAAQS) promulgated by U.S. Environmental Protection Agency (EPA) in 1997 to reflect more recent health-effect studies for ground-level O₃ are 0.08 ppm.¹ The standard is considered to be attained if the daily maximum 8-hr average O₃ concentration does not exceed 0.08 ppm more than three times in 3 years. Chameides et al.² showed that more regions in the U.S. will have daily maximum 8-hr O₃ concentrations that exceed the level of the revised NAAQS than the old standard, which is 0.12 ppm for the daily maximum 1-hr O₃. It is desirable for local air quality agencies to accurately forecast O₃ concentrations to warn the public of unhealthy air and to encourage people to voluntarily reduce emissions-producing activities.

Different air pollution forecasting systems for O₃ have been developed and are presently in operational use in the United States and other countries, ranging from simple statistical models to comprehensive three-dimensional air quality simulation models.¹ EPA¹ reviewed the definitions, strengths, and limitations of the most commonly used forecasting methods so far, including persistence, climatology, criteria, classification and regression tree, regression equations, artificial neural networks, the phenomenological/intuition method, and three-dimensional air quality models. Three-dimensional air quality forecast models have been increasingly used in operational applications because they can forecast temporal and spatial distributions of O₃ and its precursors over regions where observations are sparse and help to understand the chemical-physical processes that control O₃ in a specific area. Kang et al.³ evaluated the operational performance of three three-dimensional air quality forecast models and found that all three models tended to overestimate O₃ concentrations with mean biases (MBs) ranging from 0.53 ppb for maximum 8-hr forecast to 7.42 ppb for maximum 1-hr forecast. In this study, the National Weather Service operational mesoscale forecast Eta model is used to supply meteorological input to the EPA Models-3/Community Multi-scale Air Quality (CMAQ) model (Eta-CMAQ model suite); the models are then used to provide estimations of O₃ and related chemical species in a forecast mode. The information from the other O₃-related chemical species can help to gain an understanding of the physical and chemical processes dictating tropospheric O₃ distributions. The developmental testing of fine particulate matter forecast capability with the Eta-CMAQ model is under way.⁴ The objectives of this study are: (1) to evaluate the temporal and spatial performances of the Eta-CMAQ forecast model for O₃ against the observations from the Air Quality System (AQS) network over the Northeastern United States; and (2) to use a variety of diagnostic tests involving measurements from the 2002 New England Air Quality Study (NEAQS) to examine the ability of the Eta-CMAQ model in representing the physical and chemical processes dictating tropospheric O₃ distributions.

DESCRIPTIONS OF THE MODEL AND OBSERVATIONAL DATA

Eta-CMAQ Forecast Modeling System

The Eta-CMAQ air quality forecasting (AQF) system is based on the National Centers for Environmental Estimation (NCEP) Eta model⁵ and the EPA CMAQ Modeling System.⁶ Otte et al.⁷ describe the methodology developed to link the two modeling systems. A brief summary relevant to the present study is presented here. The Eta model is used to generate the three-dimensional meteorological fields required for the chemistry and transport calculations in the CMAQ. The NCEP Product Generator software is used to perform the bilinear interpolations and nearest-neighbor mappings of the Eta postprocessor output from the Eta forecast domain to the CMAQ forecast domain. The emissions are from EPA national emission inventory (1999 NEI v1). The Carbon Bond chemical mechanism (version 4.2) (CB-IV) is used for photochemical processes.

Detailed description of the governing equations, physical parameterizations, and numerical techniques used in the CMAQ model can be found in Byun and Ching.⁶ In this study, the modeling system is deployed over a domain covering the Northeast United States (Figure 1). A Lambert Conformal map projection is used, and the horizontal domain is discretized using grids of 12-km resolution. Twenty-two layers of variable thickness set on a σ coordinate are used to resolve the vertical extent from the surface to ~100 hPa. The lateral boundary conditions are set using horizontally constant and typically "clean" continental profiles for O₃ and other trace gases with some vertical variations based on climatology. The initial conditions for modeled chemical species are set from the previous forecast cycle. The Eta 12 UTC and 06 UTC cycles are used for the forecast cycle.⁷ The primary Eta-CMAQ model forecast for next-day surface-layer O₃ is based on the 12 UTC Eta cycle of the current day, and products are issued daily no later than 1:30 p.m. The target forecast period is local midnight through local midnight (04 UTC to 03 UTC for the Northeast United States), so in this work, the first 16-hr results of the CMAQ forecast based on the 12-UTC run are discarded. An additional 8 hr is required beyond midnight to calculate peak 8-hr average O₃ concentrations. Therefore, a 48-hr Eta-CMAQ forecast is needed on the basis of the 12-UTC initialization to obtain the desired 24-hr forecast period. The model performance from August 6 to August 17, 2002, based on the 12-UTC run for the target forecast period is evaluated in this study.

Observational Databases

Hourly O₃ data at 342 sites in the Northeast United States are available from EPA AQS network (Figure 1). The cell location of a site is used for matching the model estimations with observations. For cases in which the model grid cells contained more than one monitor, the average concentration from the monitors was used. Four Atmospheric Investigation, Regional Modeling, Analysis, and Estimation (AIRMAP) sites and Harvard Forest ([HF] 42.64° N, 72.17° W) provided continuous measurements of O₃ and related photochemical species, as well as meteorological parameters during the 2002 NEAQS. The four AIRMAP

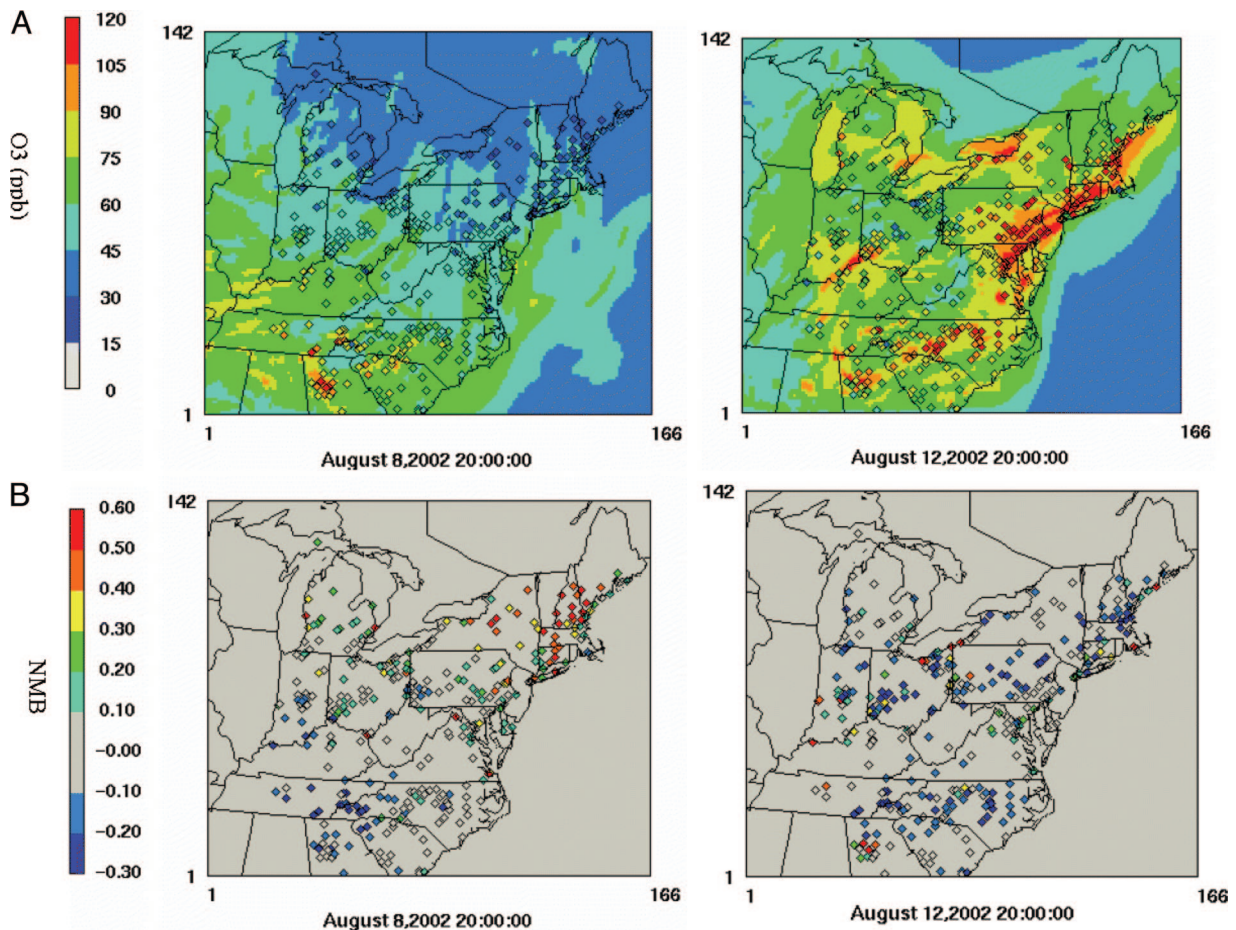


Figure 1. (A) AQF system simulation results for O_3 concentration (ppb) with AQS observed data overlaid (\diamond) and (B) the normalized MB ($NMB = [model - observed]/observed$) over the Northeastern United States at 20:00 UTC (3:00 p.m.) August 8 and 12, 2002.

sites include Castle Springs ([CS] 43.73° N, 71.33° W), Isle of Schoals ([IS] 42.99° N, 69.33° W), Mount Washington Observatory ([MWO] 44.27° N, 71.30° W), and Thompson Farm ([TF] 43.11° N, 70.95° W) sites. Both CS and TF sites are characterized by mixed hardwood/pine forest, and IS is an uninhabited ocean site (see airmap.unh.edu/). MWO is the highest mountain (1916 m) in the Northeastern United States. To compare the observations with the model estimations, the hourly averages for the observations were calculated if >50% of the 1-min observations in that hour were available. O_3 lidar vertical profiles obtained from the lidar onboard the NOAA ship Ronald H. Brown during the NEAQS 2002 (www.etl.noaa.gov/et2/data/data_pages/neaqs/opal/) were used to evaluate the model performance in the vertical. The lidar measured O_3 concentrations from 295 m to 1975 m with 30-m vertical resolution and 5-min time resolution; to compare with the model estimations, the hourly mean O_3 vertical profiles are calculated.

RESULTS AND DISCUSSION

O_3 Episode Analysis during the Simulation Period

Because the mobile sources (or urban plumes) are rich in CO and nitrogen oxide (NO_x), and point source emissions from power plants are often rich in SO_2 and NO_x , the

SO_2 /reactive odd nitrogen ($[NO_y]$ $NO_y = NO + NO_2 + NO_3 + 2*N_2O_5 + HONO + HNO_3 + PNA +$ peroxyacetyl nitrate [PAN] + NTR [an inert organic nitrogen terminal product in the CB-IV chemical mechanism]) ratios can be used to discriminate between air masses dominated by mobile sources ($SO_2/NO_y < 1$) or by point sources ($SO_2/NO_y > 1$). Figure 2 shows the time series of modeled and observed SO_2 , CO, and $(SO_2)/(NO_y)$ ratios at the CS and TF sites. As can be seen, these sites were significantly influenced by the polluted plumes from both mobile and point sources after approximately August 10, because observed CO, SO_2 , and $(SO_2)/(NO_y)$ ratios increased significantly. The model captured the buildup of SO_2 after August 10 at the CS site, whereas the model systematically overestimated the observed SO_2 mixing ratios at the CS and TF sites most of time as shown in Figure 2. One of the possible reasons for the overestimation of SO_2 comes from nonrepresentative locations and elevations of surface observation sites, because most of SO_2 is emitted from stacks (point sources) above local shallow inversion layers, with the observation stations located close to the surface below the inversions.⁸ Consequently, more rapid mixing in the model relative to reality may result in overestimation of SO_2 concentrations at these sites. On the other hand, the model captured the temporal variations of observed CO at these two sites much better than SO_2 as shown in Figure

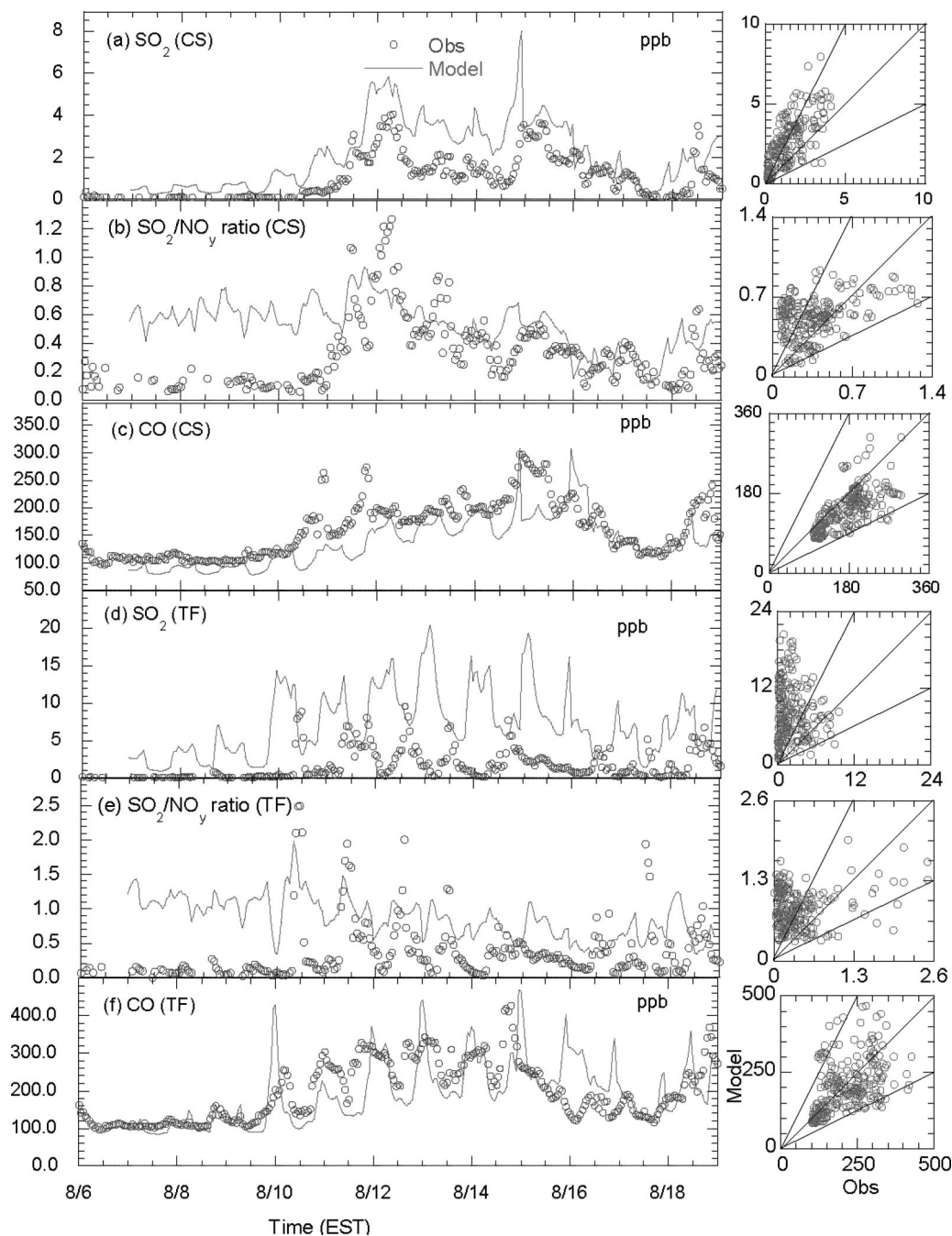


Figure 2. Time series of modeled and observed SO_2 , CO , and $[\text{SO}_2]/[\text{NO}_y]$ ratios and their scatter plots (the 2:1, 1:1, and 1:2 lines are shown for reference) at CS and TF.

2 (also see Table 2). This indicates that the model simulated the impact at these sites of mobile sources (or urban plumes) better than that from power plant point sources during this period. To contrast the regional O_3 distributions before and during the O_3 episode, Figure 1 shows comparisons of the model estimations and observations at the AQS sites for O_3 at 3:00 p.m. on August 8 and 12. The model reproduced the spatial distributions of observed O_3 very well for the daytime (3:00 p.m.) of both August 8 and 12 with most of NMB less than $\pm 20\%$. The differences in meteorological conditions between August 8 and 12 can explain why O_3 concentrations in the Northeast increased from near background concentrations on

August 8 to concentrations >100 ppb by August 12, because the emission forcings do not change significantly between these 2 days. Examination of the meteorological conditions impacting the Northeast during the August 8–13 period reveals a classic “transitional anticyclone” scenario⁹ in which a clean, cold-core continental polar air mass transitions, through continued subsidence, into a warm-core, mixing-limiting air mass that is conducive to the formation of O_3 . At the surface, both the temperature and dew point also increase (between 5 and 10 °C) as initially north/northeasterly winds veer into the south, advecting warmer, precursor-laden air from the industrialized Midwest and Ohio River Valley. The dominant SW

Table 1. Operational evaluation on the basis of the AQS data over the Northeastern United States.

Data	RMSE (ppb)	MB (ppb)	NMB (%)	NME (%)	r
Hourly	24.23	12.55	29.77	46.87	0.63
Max 1-hr	17.65	2.32	3.24	20.05	0.70
Max 8-hr	17.03	5.74	9.02	21.86	0.70

wind on August 12 placed the Northeast United States downwind of concentrated NO_x sources in the industrialized Midwest and Ohio River Valley. The buildup of the observed SO₂, CO, and (SO₂)/(NO_y) at the CS and TF sites after August 10 in Figure 2 indicates the effects of the southwesterly flow. The air masses originating from the north and influencing these sites are not affected by large anthropogenic emission sources.¹⁰

Performance Evaluation over the Northeast U.S. Domain at the AQS Sites

For the model performance evaluation, we calculated summary and regression statistics along with two measures of bias, the MB and the normalized MB (NMB), and two measures of error, the root mean square error (RMSE) and normalized mean error (NME).³ Table 1 summarizes the evaluation results for the hourly, daily maximum 1-hr and maximum 8-hr O₃ concentrations. The recommended performance criteria for O₃ by EPA are: mean normalized bias ±5 to ±15%; mean normalized gross error 30–35%; and unpaired peak estimation accuracy: ±15% to ±20%. The NMB (29.8%) and NME (46.9%) values for the hourly O₃ are higher than those performance criteria. The NMB and NME values for maximum 1-hr (maximum 8-hr) O₃ are 3.2% (9%) and 20.1% (21.9%), respectively, close to the performance criteria for the unpaired peak O₃. Scatter plot of Figure 3A indicates that the model reproduced a majority of the observed maximum 1-hr (88.6%) and maximum 8-hr O₃ (83%) within a factor of 1.5. The model generally overestimated at the low-observed O₃ concentration ranges but underestimated at the high-observed O₃ concentration ranges (see Figure 3A). The overestimations at the low O₃ concentration range are, in part, because of the assumed lateral boundary conditions of 40 ppb that result in relatively higher simulated background O₃ levels. A closer inspection reveals that most of sites with MB > 40 ppb and estimated (or observed) O₃ concentration < 50 ppb for the maximum 8-hr O₃ in Figure 3A are located within the metropolitan regions along the Washington, DC/New York, NY/Boston, MA urban corridor as shown in Figure 3B. This means that the model did not titrate O₃ enough at the urban sites, causing the overestimations at the low O₃ concentration range. It was found that correlation coefficients (r) are between 0.5 and 0.75 at a majority of the sites with higher correlations for the maximum 1-hr and maximum 8-hr compared with the hourly estimations. In general, at sites with higher errors and bias, the model also shows poorer correlation with the observations. The time series of comparisons (data not shown) indicate that the model captured the domain mean observed hourly O₃ concentrations very well during the

daytime (7:00 a.m. to 4:00 p.m.) but consistently overestimated the observations during the other times (5:00 p.m. to 6:00 a.m.). Daily variations of modeled bias in Figure 3b reveal that the model overestimated (hourly, maximum 1-hr and 8-hr) at the beginning and ending dates of the study period with better performance during the middle part of the simulation. One of the reasons for this is that the O₃ concentrations in the middle part of the simulation (from August 11 to August 16) were much higher than at the beginning and ending dates.

Diagnostic Evaluation during the 2002 NEAQS

Time Series Comparison at the AIRMAP and Harvard Forest Sites. As examples, Figures 4–6 show time series comparisons and scatter plots of the model estimations and observations for O₃, NO, NO₂, CO, NO_y, PAN, NO₂ photolysis rates (J_{NO2}), and meteorological parameters at the CS and HF sites (time series of CO and SO₂ at CS and TF sites are shown in Figure 2). Table 2 summarizes the statistical results for the model evaluations at the AIRMAP and HF sites. Following Yu et al.,⁸ the percentages of the comparison points where the model results are within a factor of 1.5 and 2, respectively, of the observations are listed in Table 2. Here, factor is defined as ratio of model estimation to observation if the model estimation is higher than the observation, whereas it is defined as ratio of observation to model estimation if the observation is higher than the model estimation. The model captured the hourly variations and broad synoptic changes seen in the observations of different gas species (O₃, CO, NO_y, and PAN; correlation coefficient > 0.50; see Table 2) except NO and SO₂ at each site. For O₃, the model reproduced the general temporal variations most of the time at all sites (>58% within a factor of 1.5 and >75% within a factor of 2; r > 0.69; see Table 2) with better performance at the HF and MWO sites. The model estimations for NO are noticeably worse with underestimations of the observations most of the time at the CS and MWO sites, in part, possibly reflecting the inherent subgrid variability in NO emissions and concentrations that are not adequately captured by the model grid resolution. The model performance for CO at all of the sites is very good, with >90% of the comparisons within a factor of 2. For NO_y, the model reproduced 76.7%, 74.1%, and 51.6% of observations within a factor of 2 at the CS, HF, and TF sites, respectively, but the model mean NO_y concentrations are systematically ~50% higher than the observations at all three of the sites (see Table 2). A closer inspection of Figures 4 and 6 reveals that overestimations of peak NO_y at the CS and HF sites occur during the nighttime with the largest contribution by HNO₃ (~20–60%) and followed by NTR (~10–40%). In the CB-IV chemical mechanism, the species NTR represents an inert organic nitrogen terminal product. There are several reasons for these nighttime NO_y overestimations, including: (1) the relatively coarse vertical resolution of the model that cannot adequately resolve sharp nocturnal gradients near the surface; (2) uncertainties associated with atmospheric sinks for the modeled organic nitrate species represented by NTR; and (3) overestimation of the gas-phase hydrolysis reaction of N₂O₅ with water, which produces too much

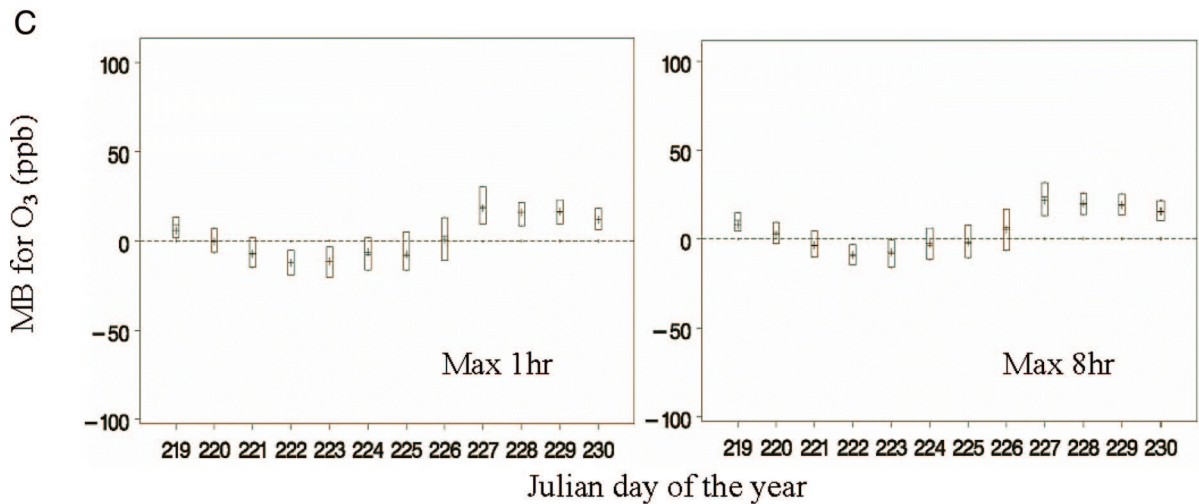
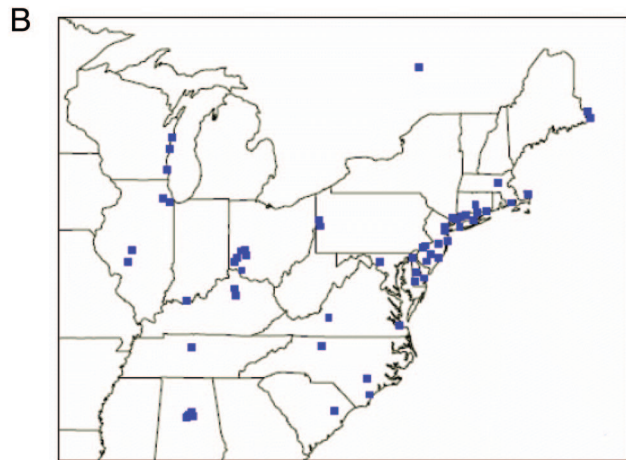
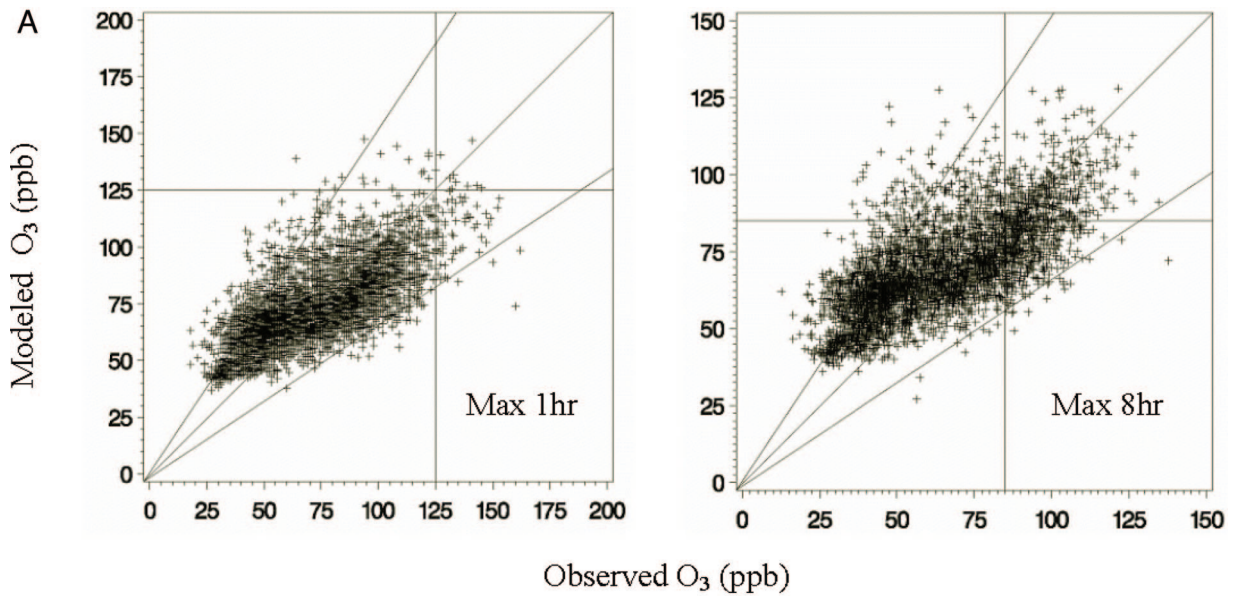


Figure 3. (A) Scatter plots between the models and observations for maximum 1-hr and maximum 8-hr O₃ concentrations with exceedance thresholds and 1:1.5, 1:1, and 1.5:1 lines indicated at the AQS sites. (B) Locations with maximum 8-hr O₃ concentrations <50 ppb and MB >40 ppb. (C) Boxplots (denoting 75th, 50th, and 25th percentiles) for daily MB (MB = Model-Obs) for maximum 1-hr and maximum 8-hr O₃ concentrations over the domain.

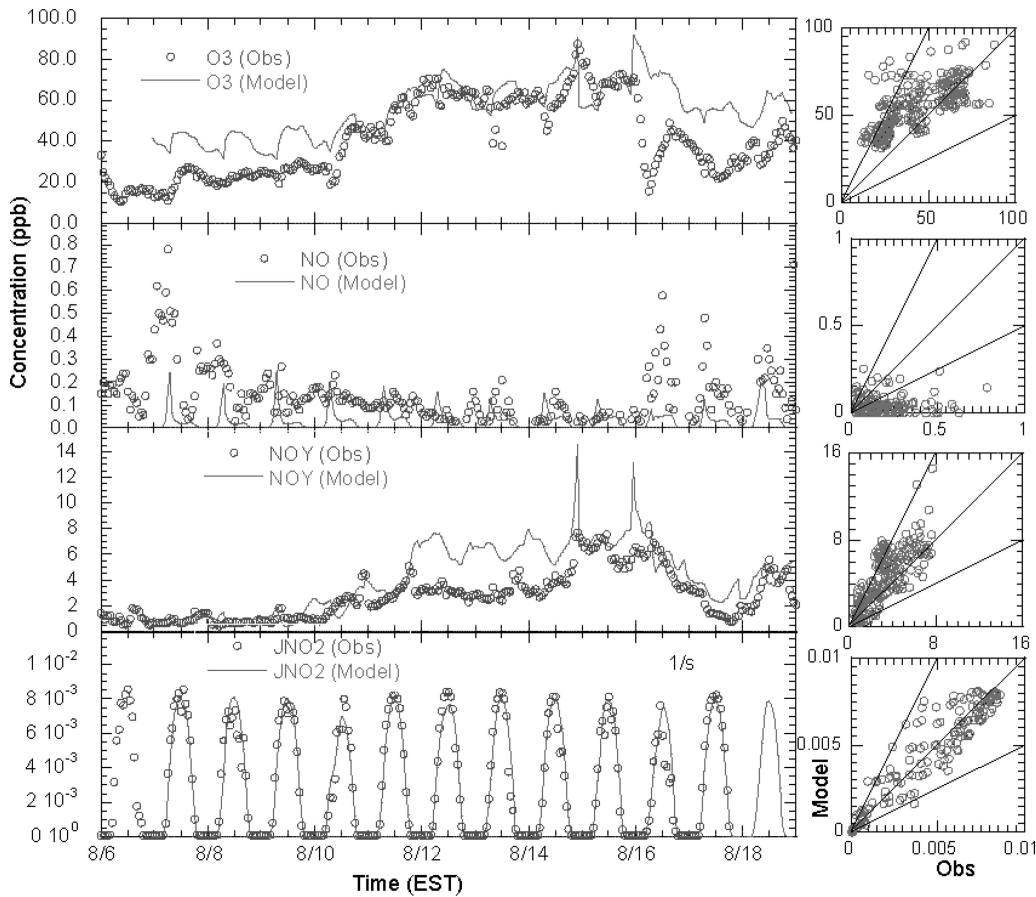
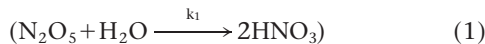


Figure 4. Time series and scatter plots (the 2:1, 1:1, and 1:2 lines are shown for reference) of model estimations and observations at the CS site.

nighttime HNO_3 in the CB-IV chemical mechanism. Although it is generally believed that the reaction of N_2O_5 with water



is a major sink of NO_x in the troposphere during the nighttime, the importance of this reaction is still a subject of scientific debate. Atkinson et al.,¹¹ for instance, suspected that this N_2O_5 homogeneous hydrolysis reaction does not exist at all. The CB-IV k_1 value of $1.3 \times 10^{-21} \text{ cm}^3 \text{ molec.}^{-1} \text{ sec}^{-1}$ is close to upper limits of $1.3\text{--}1.5 \times$

$10^{-21} \text{ cm}^3 \text{ molec.}^{-1} \text{ sec}^{-1}$ obtained from smog chamber studies^{11,12} but up to a factor of 5 larger than those ($0.3\text{--}1 \times 10^{-21} \text{ cm}^3 \text{ molec.}^{-1} \text{ sec}^{-1}$) obtained by atmospheric NO_3 measurements.¹³ The laboratory measurements of Wahner et al.¹⁴ found that the k_1 value was $2.5 \times 10^{-22} \text{ cm}^3 \text{ molec.}^{-1} \text{ sec}^{-1}$ with a third-order reaction:

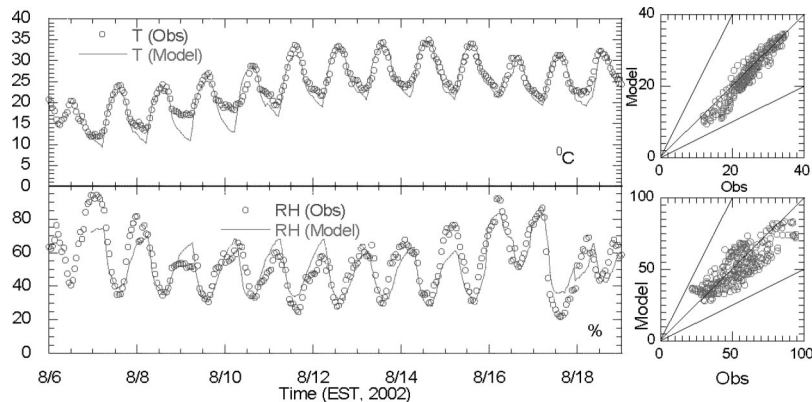
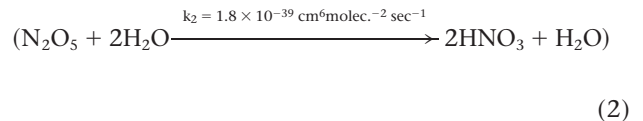


Figure 5. Same as Figure 4 but for meteorological conditions at the CS site. The 2:1, 1:1, and 1:2 lines are also shown for reference in the scatter plots.

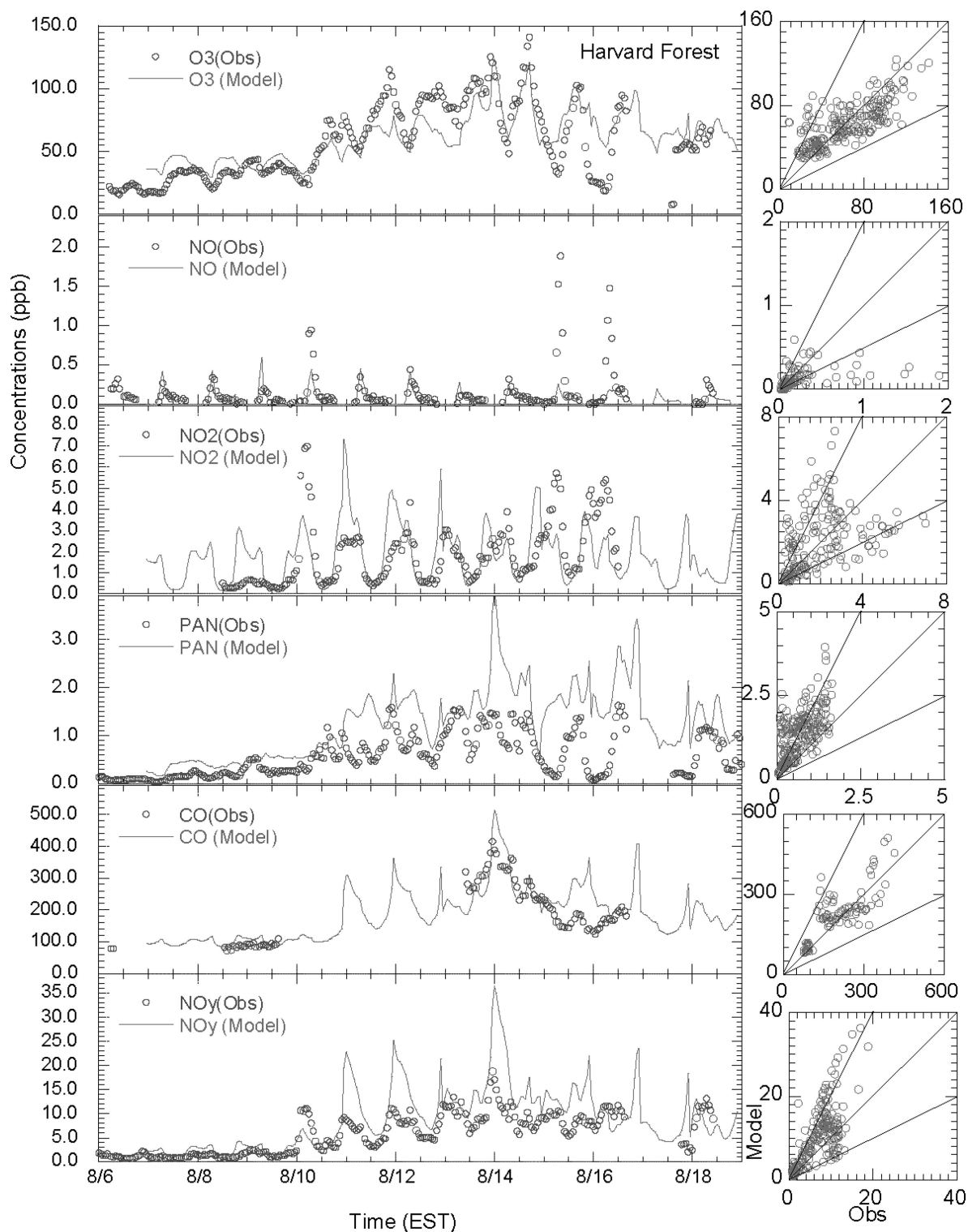
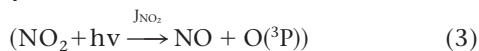


Figure 6. Same as Figure 4 but at the HF site. The 2:1, 1:1, and 1:2 lines are also shown for reference in the scatter plots.

Clearly, the high value of k_1 in the model results in overestimation of nighttime HNO_3 formation, mainly causing the overprediction of nighttime NO_y shown in Figures 4 and 6.

The photolysis rates of NO_2



at the CS, MWO, and TF sites were measured during the 2002 NEAQS. Following Thornton et al.,¹⁵ we focus our

analysis on daylight hours by excluding data where $J_{\text{NO}_2} < 5 \times 10^{-5} \text{ sec}^{-1}$. As shown in Figure 4 and Table 2, the model reproduced the diurnal variations of observed J_{NO_2} at each site very well, with $r > 0.92$. Table 2 indicates that the model reproduced 77.1%, 64%, and 70.9% of observed J_{NO_2} values within a factor of 1.5 at the CS, MWO, and TF sites, respectively. Demore et al.¹⁶ suggest that in computing J_{NO_2} values, as much as

Table 2. Statistical summaries of the comparisons of the model results with the observations at the different sites during the 2002 NEAQS.

Parameters	<C> ^a		<i>r</i>	% Within a Factor of 1.5 ^b	% Within a Factor of 2 ^b
	Observed	Model			
CS (<i>N</i> = 288)					
O ₃	42.94	55.21	0.695	58.7	86.5
NO	0.15	0.03	0.172	9.3	18.1
CO	166.31	137.96	0.724	86.5	99.0
NO _Y	2.91	4.15	0.800	46.5	76.7
SO ₂	1.29	2.46	0.751	23.4	44.7
J _{NO2} (1/sec)	4.37 × 10 ⁻³	4.40 × 10 ⁻³	0.971	77.1	91.4
Temperature (C)	24.61	23.59	0.962	99.0	100.0
RH (%)	53.22	51.23	0.843	98.6	100.0
HF (<i>N</i> = 288)					
O ₃	60.01	60.26	0.773	80.8	92.0
NO	0.16	0.09	0.467	36.8	55.6
NO ₂	1.85	1.97	0.443	38.4	60.5
CO	197.75	220.55	0.804	87.8	98.0
NO _Y	6.10	9.20	0.766	40.1	74.1
PAN	0.62	1.23	0.690	24.2	47.2
RH (%)	74.08	60.65	0.882	96.6	100.0
IS (<i>N</i> = 288)					
O ₃	56.33	69.00	0.733	65.3	86.1
CO	237.93	168.00	0.631	48.1	90.6
MWO (<i>N</i> = 288)					
O ₃	60.65	53.11	0.827	86.3	99.3
NO	0.24	0.02	0.066	12.4	23.2
CO	154.59	119.68	0.639	82.7	96.0
SO ₂	1.23	1.52	0.662	33.2	48.4
J _{NO2} (1/sec)	4.01 × 10 ⁻³	4.72 × 10 ⁻³	0.917	64.0	77.7
TF (<i>N</i> = 288)					
O ₃	44.39	56.74	0.819	59.0	76.0
NO	0.16	0.19	0.636	23.7	42.0
CO	203.46	194.24	0.550	80.5	92.7
NO _Y	4.60	9.51	0.505	25.1	51.6
SO ₂	1.94	7.64	0.028	13.8	18.5
J _{NO2} (1/sec)	4.32 × 10 ⁻³	4.24 × 10 ⁻³	0.944	70.9	86.3
Temperature (C)	24.09	24.40	0.942	100.0	100.0
RH (%)	64.26	55.38	0.834	92.0	100.0

Notes: *r* is correlation coefficient between the model predictions and observations; ^a <C> is the mean concentration (ppb); ^b Percentages (%) are the percentages of the comparison points at which model results are within a factor of 1.5 and 2 of the observations.

±20% uncertainty can arise because of uncertainties in the cross-section and quantum yield data. Additional uncertainties in the model simulations can also arise from uncertainties and errors associated with the spatial and temporal representation of cloud fields in the model and their subsequent effects on photolysis attenuation.

Figure 5 shows that the model reproduced the temporal variations of the observed temperatures and relative humidity (RH) at the CS site very well. The modeled mean temperatures (RH) at the CS and TF are 23.59 °C (51.23%) and 24.40 °C (55.4%), respectively, very close to the observations with ~±5% errors for temperature and ~±10% for RH as shown Table 2.

Evaluation of O₃ Vertical Profiles against Lidar Data. Diurnal variations in surface O₃ concentrations have been found to be associated with residual O₃ aloft.^{17,18} Berkowitz et al.¹⁷ showed that these elevated photochemically

aged layers frequently formed over the Northeastern United States during the summer and that turbulent mixing and transport led to the formation of these layers. Comparisons of modeled and ship-based lidar measurements of vertical profiles provide an assessment of the ability of the model to represent vertical structure of O₃ distributions. Figure 7, a and b, presents comparisons of modeled and observed time-height variations in O₃ structure along the ship tracks (see Figure 7d) during the period of August 7–10, 2002. The scatter plots between the observations and model estimations for individual values and model-layer means are shown in Figure 7c. As can be seen, the model captured most of the observations (70%) within a factor of 1.5, especially for the layer means (71%). The model reproduced the observed O₃ concentrations reasonably well at the lower altitudes between 355 and 500 m, especially after August 9, as shown in Figure 7. The mean model estimation at these altitudes (56.9 ± 8.3

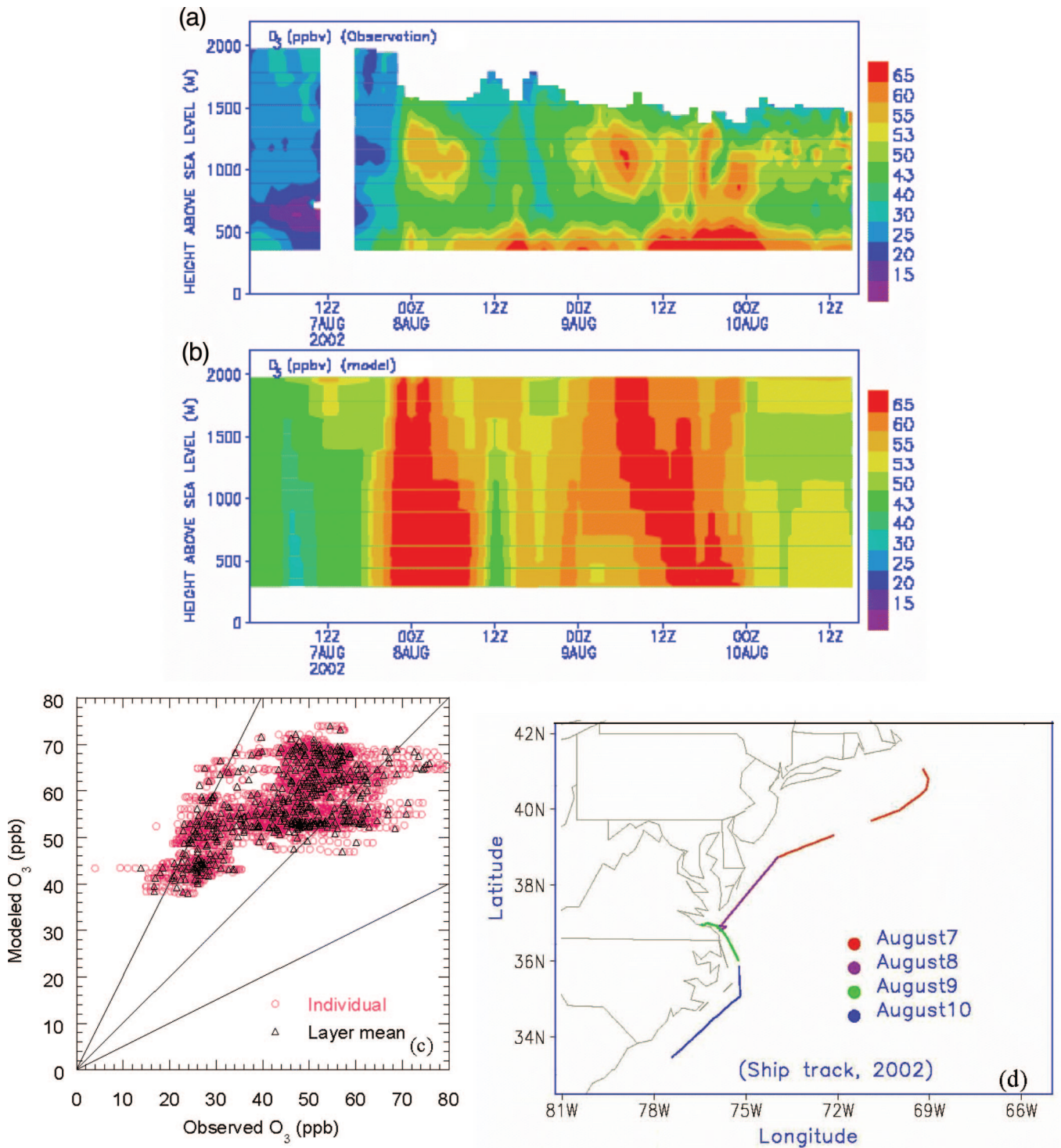


Figure 7. Vertical O₃ profiles for the (a) lidar observations and (b) model during the period from August 7 to 10, 2002. (c) is a scatter plot between the observations and model estimations for individual value and model-layer means (the 2:1, 1:1, and 1:2 lines are shown for reference), and (d) shows ship tracks.

ppb) is in good agreement with the observation (55.0 ± 13.7 ppb). However, relative to the complex observed structures, the modeled vertical distributions of O₃ are more uniform with a tendency to overestimate at higher altitudes as shown in Figure 7.

O₃ and CO Relationships in the Photochemically Aged Air at Each Site. Because CO is a long-lived tracer of human activity with well-known sources from combustion, industry, mobile, and oxidation of hydrocarbons, O₃-CO correlations have in the past been used to diagnose

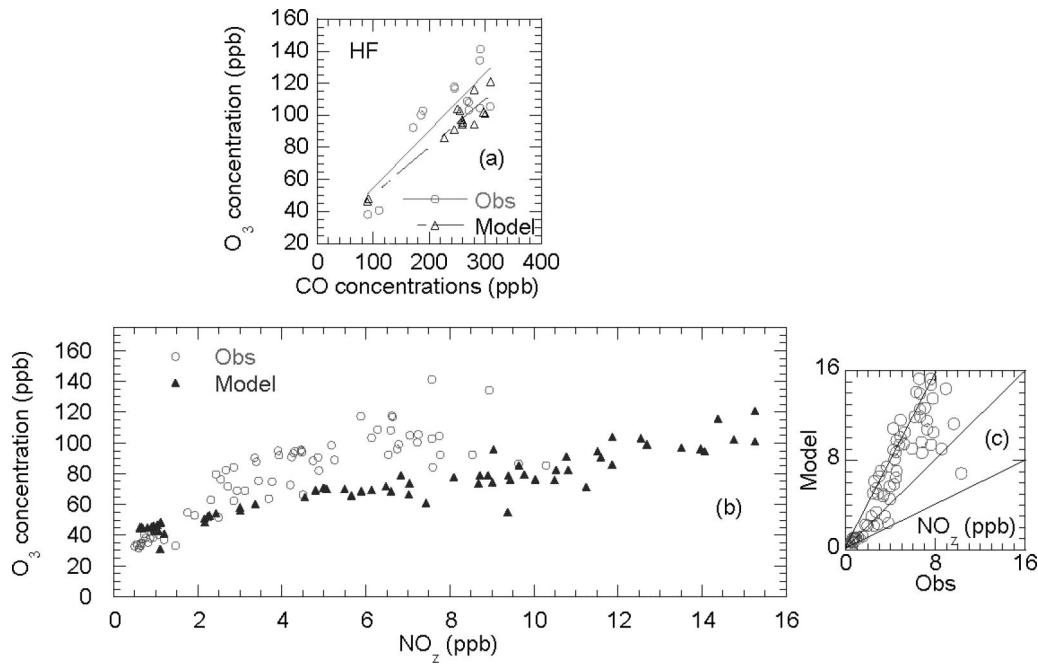


Figure 8. (a) O₃-CO correlations for the model estimations and observations for the daytime period from 1:00 to 5:00 p.m.; (b) O₃ as a function of NO_z for the NO_x-limited conditions indicated by the observational data with [O₃]/[NO_x]>46 at the HF site and scatter plot between model and observation for NO_z.

pollution influence of anthropogenic sources on O₃.¹⁹ Following Chin et al.,¹⁹ we only used the observed data with NO_x/NO_y < 0.3 (photochemically aged rural air) and between the period from 1:00 to 5:00 p.m., when surface air is most likely representative of the boundary layer. With this selection criterion, only data for the period August 10–15 when the sites were mainly influenced by the southwesterly flow as analyzed in the previous section were left. As shown in Figure 8a and Table 3, there are strong correlations (correlation coefficient >0.86) between O₃ and CO for both model estimations and observations at the HF site. The slope (ΔO₃/ΔCO) is 0.29 for the model estimation, close to

that from the observation (0.36; see Table 3). This is in agreement with Chin et al.,¹⁹ who found that ΔO₃/ΔCO ≈ 0.3 was a uniform characteristic of boundary layer air over eastern North America in summer. The analyses of O₃ and CO at TF and CS over 2 years (2001–1003) by Mao and Talbot²⁰ reveal that in summer during the local afternoon (1:00–6:00 p.m.) a well-defined positive O₃-CO correlation with a slope ~0.37 existed in the air masses from the southeasterly and westerly wind sectors. Our results are also in agreement with their findings. As analyzed by Chin et al.,¹⁹ a lower limit for the net O₃ production efficiency (ε_N, defined as the net number of O₃ molecules produced per molecule

Table 3. Summary of results at the HF site.

Sites	O ₃ -CO Correlation Equations	Correlation Coefficient
O ₃ -CO correlation equations (N = 14) ^a		
Observation	O ₃ = 18.69 + 0.36CO	r = 0.857
Model	O ₃ = 20.76 + 0.29CO	r = 0.950
O ₃ -NO _z correlation equations (N = 82) ^b		
Observation	[O ₃] = 9.1[NO _z] + 39.5	r = 0.849
Model	[O ₃] = 4.2[NO _z] + 41.9	r = 0.942
No. of hours for the different O ₃ /NO _x bins ^c		
0–14	28 (21) ^d	16 (12) ^e
15–25	11 (8) ^d	26 (20) ^e
26–45	11 (8) ^d	20 (15) ^e
>46	83 (62) ^d	71 (53) ^e
Total hours	133 (100) ^d	133 (100) ^e

Notes: ^aO₃-CO correlations in photochemically aged air (as defined by the observed NO_x/NO_y<0.3) for the daytime period from 1:00 to 5:00 p.m.; ^bCorrelations between O₃ and NO_z for the NO_x-limited conditions indicated by the observational data with [O₃]/[NO_x]>46 (aged air masses); ^cStatistical summary of number of hours for response surface indicator ratios (O₃/NO_x) for model and observations for all days (observed-limited hours; the values in parentheses are the percentages) at the HF site during the period of August 6–17, 2002; ^dObservations; ^eModel.

of NO_x consumed) can be estimated by scaling the slope $\Delta\text{O}_3/\Delta\text{CO}$ in the photochemically aged air to a CO/NO_x source ratio. Such an estimate is a lower limit because of deposition of O_3 . According to EPA emission inventory used in the model, the mean value of the CO/NO_x emission ratio over the Midwest (the upwind region of the site) is 8.5 ± 2.9 , yielding estimated ϵ_N lower limit values of 2.5 ± 0.8 for the model and 3.1 ± 1.0 for the observation.

Comparison of Modeled and Observed NO_x -Sensitive Chemical Regimes, Air Mass Photochemical Age, and O_3 Production Efficiencies at the HF Site. Analyses of indicator ratios (i.e., $[\text{O}_3]/[\text{NO}_x]$, $[\text{NO}_z]/[\text{NO}_y]$, and $[\text{O}_3]/[\text{NO}_z]$) can be used to evaluate the model performance in determining NO_x -sensitive and volatile organic compound (VOC)-sensitive chemical regimes, air mass photochemical ages, and O_3 production efficiency. Following Tonnesen and Dennis²¹ and Arnold et al.,²² the total hours spent in each extreme region and nearer to the $[\text{O}_3]$ ridgeline according to the $[\text{O}_3]/[\text{NO}_x]$ values are calculated and listed in Table 3 for the HF site. $[\text{O}_3]/[\text{NO}_x]$ values >46 indicate strong NO_x -sensitive conditions, whereas values <14 indicate VOC-sensitive conditions, which are often prevalent at the surface during peak morning commutes or in fresh power plant plumes.²² Table 3 reveals that for the most part, the model correctly reproduced the temporal variations in the observed $[\text{O}_3]/[\text{NO}_x]$ ratios across the different conditions represented at the HF site. For example, both model and observations show that the site is mainly under strongly NO_x -sensitive conditions ($\geq 53\%$; see Table 3).

The fraction of NO_y converted to NO_z can be used to represent the air mass photochemical age. $[\text{NO}_z]/[\text{NO}_y]$ values <0.6 indicate a fresher NO_x plume with an increased potential for O_3 production or loss, conditional on radical availability in the system, whereas higher $[\text{NO}_z]/[\text{NO}_y]$ values indicate an aged air mass with less potential for change in O_3 .²² The air mass photochemical age approaches unity as NO_x is completely oxidized. It is found that the percentage of the daytime (6:00 a.m. to 6:00 p.m.) hours with air mass photochemical age values $[\text{NO}_z]/[\text{NO}_y] >0.6$ for the model is 87% at the HF site, close to the corresponding observed values of 82% at the HF site. These findings are similar to those reported by Olszyna et al.,²³ who found that $>70\%$ of the midday ratios were >0.6 at a rural site in the Eastern United States.

The O_3 production efficiency (ϵ_N), that is, the number of O_3 molecules produced for each NO_x molecule processed to NO_z , can be estimated by the slope of the O_3 - NO_z correlation. Following Arnold et al.,²² both modeled and observed O_3 - NO_z slopes are obtained for only observational data with $[\text{O}_3]/[\text{NO}_x] >46$ during the daytime (6:00 a.m. to 6:00 p.m.) at the HF site to ensure that the system is well out of the radical-sensitive region of the response surface. Table 3 indicates that there is significant correlation between O_3 and NO_z for both model estimations and observations ($r > 0.77$; also see Figure 8). Note that the data during the nighttime corresponding to the NO_y overestimations shown in Figure 6 are automatically not included in the O_3 - NO_z analysis for Figure 8 and Table 3 when the above-mentioned screening criteria are used. The modeled ϵ_N value (4.2) at the HF site is close ($\sim 16\%$

lower) to the lower bound of the estimated range (5–10) of other investigators²³ at rural sites in the Eastern United States. In contrast, the observed ϵ_N value (9.1) is close to the higher bound of the estimated range of other investigators. The modeled intercept is slightly higher than the observations. Chin et al.²⁰ suggest that the ϵ_N values estimated by the O_3 - NO_z slopes are upper limits, because NO_z species (primarily HNO_3) are removed from the atmosphere more rapidly than O_3 . Figure 8 shows that compared with the observations, the model produced less O_3 at the high NO_z regime. The scatter plots of Figure 8 also show that the modeled NO_z concentrations were higher than the observations, indicating that the model chemistry produces more terminal oxidized nitrogen products than inferred from observations, thereby contributing to the noted underestimation of ϵ_N .

CONCLUSIONS

The Eta-CMAQ AQF system has been developed and applied to forecast O_3 over the Northeastern United States during the 2002 NEAQS. The episode analysis reveals that the model captured the buildup of O_3 concentrations over the NE domain from August 10 and reproduced the spatial distributions of observed O_3 very well for the daytime (3:00 p.m.) for both regional low (August 8) and high (August 12) with NMB values at most sites within $\pm 20\%$. On the basis of the evaluation at the 342 AQS sites, it is found that the model reproduced 53% of observed hourly O_3 within a factor of 1.5 with domain-wide NMB of 29.7% and NME of 46.9%. The comparison of modeled and lidar-based observed O_3 vertical profiles shows that whereas the model reproduced the observed O_3 concentrations well at the lower altitudes between 355 and 500 m, it tended to overestimate at higher altitudes. On the basis of the evaluation results at the four AIRMAP and HF sites, it was found that the model captured the hourly variations and broad synoptic and interday variations seen in the observations of different gas species (O_3 , NO_2 , CO , NO_y , PAN, and SO_2). The model reproduced 77.1%, 64%, and 70.9% of observed J_{NO_2} values within a factor of 1.5 at the CS, MWO, and TF sites, respectively. On the basis of results at the HF site, it is found that both models and observations show that the site is mainly under strongly NO_x -sensitive conditions ($>53\%$). The percentage of daytime (6:00 a.m. to 6:00 p.m.) hours when the HF site was influenced by relatively chemically mature plumes ($[\text{NO}_z]/[\text{NO}_y] >0.6$) is close to that of the observations. The modeled lower limits of the O_3 production efficiency (ϵ_N) value (2.9) are slightly lower than the observation (3.6) at the HF site estimated on the basis of relationship between O_3 and CO . However, the modeled upper limit (4.2) of the ϵ_N values estimated by the O_3 - NO_z slopes is about half of the observations (9.1). There are uncertainties in the photochemical mechanism, emission inventories, and prognostic model forecasts of meteorological fields for real time. In light of these uncertainties and difficulties, the performance of the Eta-CMAQ forecast model for O_3 over the Northeastern U.S. domain can be considered to be reasonable. The performance of the Eta-CMAQ forecast model over the past 3 summers is also being continuously evaluated. Detailed analyses of model estimations against extensive datasets collected during

the 2004 NEAQS campaign are under way and will provide additional evaluation of the model's estimative capability for tropospheric O₃ distributions.

ACKNOWLEDGMENTS

The authors thank three anonymous reviewers, Drs Robin Dennis, Gerald Gipson, and Patrick Dolwick, for the constructive and very helpful comments that led to a substantial strengthening of the content of the paper. We are grateful to the 2002 NEAQS investigators for making their measurement data available and thank NOAA Environmental Technology Laboratory for several helpful discussions on the lidar O₃ vertical profiles. The research presented here was performed under the Memorandum of Understanding between EPA and the U.S. Department of Commerce NOAA and under agreement number DW13921548. This work constitutes a contribution to the NOAA Air Quality Program. Although it has been reviewed by EPA and NOAA and approved for publication, it does not necessarily reflect their policies or views.

REFERENCES

1. *Guideline for Developing Ozone Forecasting Program*; EPA-454/R-99-009; U.S. Environmental Protection Agency: Research Triangle Park, NC, 1999.
2. Chameides, W.L.; Saylor, R.D.; Cowling, E.B. Ozone Pollution in the Rural United States and the New NAAQS; *Science* **1997**, *276*, 916.
3. Kang, K.; Eder, B.K.; Stein, A.F.; Grell, G.A.; Peckham, S.E.; Mchenry, J. The New England Air Quality Forecasting Pilot Program: Development of an Evaluation Protocol and Performance Benchmark; *J. Air & Waste Manage. Assoc.* **2005**, *55*, 1782-1796.
4. Mathur, R.; Kang, D.; Yu, S.C.; Schere, K.L.; Pleim, J.; Young, J.; Pouliot, G.; Otte, T. Atmospheric Particulate Matter Forecasts with the Eta-CMAQ Modeling System: towards Development of a Real-Time System and Assessment of Model Performance. Presentation at the 4th Annual CMAS Models-3 Users' Conference, September 26-28, 2005, UNC-Chapel Hill, Chapel Hill, NC; available at http://www.cmascenter.org/conference/2005/ppt/1_11.pdf.
5. Rogers, E.; Black, T.; Deaven, D.; Dimego, G.; Zhao, Q.; Baldwin, M.; Junker, N.; Lin, Y. Changes to the Operational "Early" Eta Analysis/Forecast System at the National Centers for Environmental Estimation; *Weather Forecast* **1996**, *11*, 391-413.
6. Byun, D.W.; Ching, J.K.S., Eds.; *Science Algorithms of the EPA Models-3 Community Multi-Scale Air Quality (CMAQ) Modeling System*; EPA/600/R-99/030; Office of Research and Development, U.S. Environmental Protection Agency: Research Triangle Park, NC, 1999.
7. Otte, T.L.; Pouliot, G.; Pleim, J.E.; Young, J.O.; Schere, K.L.; Wong, D.C.; Lee, P.C.S.; Tsidulko, M.; McQueen, J.T.; Davidson, P.; Mathur, R.; Chuang, H.-Y.; Dimego, G.; Seaman, N.L. Linking the Eta Model with the Community Multiscale Air Quality (CMAQ) Modeling System to Build a Real-Time National Air Quality Forecasting System; *Weather Forecast* **2005**, *20*, 367-384.
8. Yu, S.C.; Kasibhatla, P.S.; Wright, D.L.; Schwartz, S.E.; McGraw, R.; Deng, A. Moment-Based Simulation of Microphysical Properties of Sulfate Aerosols in the Eastern United States: Model Description, Evaluation and Regional Analysis; *J. Geophys. Res.* **2003**, *108*, 4353.
9. Eder, B.K.; Davis, J.M.; Bloomfield, P. An Automated Classification Scheme Designed to Better Elucidate the Dependence of Ozone on Meteorology; *J. Appl. Meteorol.* **1994**, *33*, 1182-1199.
10. Griffin, R.J.; Johnson, C.A.; Talbot, R.W.; Mao, H.; Russo, R.S.; Zhou, Y.; Sive, B.C. Quantification of Ozone Formation Metrics at Thompson Farm during the New England Air Quality Study (NEAQS) 2002; *J. Geophys. Res.* **2004**, *109*(D24302), DOI 10.1029/2004JD005344.
11. Atkinson, R.; Tuazon, E.C.; Macleod, H.; Aschmann, S.M.; Winer, A.W. The Gas-Phase Reaction of Chlorine Nitrate with Water Vapor; *Geophys. Res. Lett.* **1986**, *13*, 117-120.
12. Hjorth, J.; Ottobriani, G.; Cappellani, F.; Restelli, G. A Fourier Transform Infrared Study of the Rate Constant of the Homogeneous Gas-Phase Reaction N₂O₅+H₂O and Determination of Absolute Infrared Band Intensities of N₂O₅ and HNO₃; *J. Phys. Chem.* **1987**, *91*, 1565-1568.
13. Atkinson, R.; Winer, A.W.; Pitts, J.N. Estimation of Nighttime N₂O₅ Concentrations from Ambient NO₂ and NO₃ Radical Concentrations in and the Role of N₂O₅ in Night-Time Chemistry; *Atmos. Environ.* **1986**, *20*, 331-339.
14. Wahner, A.; Mentel, T.F.; Sohn, M. Gas-Phase Reaction of N₂O₅ with Water Vapor: Importance of Heterogeneous Hydrolysis of N₂O₅ and Surface Desorption of HNO₃ in a Large Teflon Chamber; *Geophys. Res. Lett.* **1998**, *25*, 2169-2172.
15. Thornton, J.A.; Wooldridge, P.J.; Cohen, R.C.; Martinez, M.; Harder, H.; Brune, W.H.; Williams, E.J.; Roberts, J.M.; Fehsenfeld, F.C.; Hall, S.R.; Shetter, R.E.; Wert, B.P.; Fried, A. Ozone Production Rates as a Function of NO_x Abundances and HO_x Production Rates in the Nashville Urban Plume. *J. Geophys. Res.* **2002**, *107*, DOI 10.1029/2001JD00932.
16. Demore, W.B.; Sander, S.P.; Howard, C.J.; Ravishankara, A.R.; Golden, D.M.; Kolb, C.E.; Hampson, R.F.; Kurylo, M.J.; Molina, M.J. *Chemical Kinetics and Photochemical Data for Use in Stratospheric Modeling*; Evaluation 12; NASA Jet Propulsion Laboratory, California Institute of Technology: Pasadena, CA, 1997.
17. Berkowitz, C.M.; Fast, J.D.; Springston, S.R.; Larson, R.J.; Spicer, C.W.; Doskey, P.V.; Hubbe, J.M.; Plastringe, R. Formation Mechanisms and Chemical Characteristics of Elevated Photochemical Layers over the Northeast United States. *J. Geophys. Res.* **1998**, *103*, 10631-10647.
18. Aneja, V.P.; Mathur, R.; Arya, S.P.; Li, Y.; Murray, G.C.; Manuszak, T.L. Coupling the Vertical Distribution of Ozone in the Atmospheric Boundary Layer; *Environ. Sci. Technol.* **2000**, *34*, 2324-2329.
19. Chin, M.; Jacob, D.J.; Munger, J.W.; Parrish, D.D.; Doddridge, B.G. Relationship of Ozone and Carbon Monoxide over North America; *J. Geophys. Res.* **1994**, *99*, 14565-14573.
20. Mao, H.; Talbot, R. O₃ and CO in New England: Temporal Variations and Relationships; *J. Geophys. Res.* **2004**, *109*.
21. Tonnesen, G.S.; Dennis, R.L. Analysis of Radical Propagation Efficiency to Assess Ozone Sensitivity to Hydrocarbons and NO_x: Part II: Long-Lived Species as Indicators or Ozone Concentration Sensitivity; *J. Geophys. Res.* **2000**, *105*, 9227-9241.
22. Arnold, J.R.; Dennis, R.L.; Tonnesen, G.S. Diagnostic Evaluation of Numerical Air Quality Models with Specialized Ambient Observations: Testing the Community Multiscale Air Quality Modeling System (CMAQ) at Selected SOS 95 Ground Sites; *Atmos. Environ.* **2003**, *37*, 1185-1198.
23. Olszyna, K.J.; Bailey, E.M.; Simonaitis, R.; Meagher, J.F. O₃ and NO_y Relationships at a Rural Site; *J. Geophys. Res.* **1994**, *99*, 14557-14563.

About the Authors

Shaocai Yu, Rohit Mathur, Daiwen Kang, Kenneth Schere, Brian Eder, and Jonathan Pleim are members of National Oceanic and Atmospheric Administration Air Resources Laboratory. Rohit Mathur, Kenneth Schere, Brian Eder, and Jonathan Pleim are currently on assignment from the National Exposure Research Laboratory, U.S. Environmental Protection Agency. Shaocai Yu and Daiwen Kang are currently on assignment from Science and Technology Corp. Address correspondence to: Shaocai Yu, Atmospheric Sciences Modeling Division, National Exposure Research Laboratory (NERL), U.S. Environmental Protection Agency, Research Triangle Park, NC 27711; phone: +1-919-541-0362; fax: +1-919-541-1379; e-mail: yu.shaocai@epa.gov.